AIMS Geosciences

AIMS Geosciences, 10(2): 274–289.
DOI: 10.3934/geosci.2024016
Received: 05 January 2024
Revised: 01 April 2024
Accepted: 08 April 2024
Published: 25 April 2024

https://www.aimspress.com/journal/geosciences

*Letter*

# At-rest lateral earth pressure coefficient under narrow backfill widths: A numerical investigation

**Ningxin Weng[1], Lei Fan[1,*], Cheng Zhang[1], Guobin Gong[1] and Lihua Tan[2]**

[1] Department of Civil Engineering, Xi'an Jiaotong-Liverpool University, Suzhou, China
[2] ARTS Group Co., Ltd., Suzhou, 215213, China

* **Correspondence:** Email: Lei.Fan@xjtlu.edu.cn; Tel: +86-(0)512-81883231.

**Abstract:** The lateral earth pressure at rest is typically considered in situations where lateral wall movements are negligible. Determining the coefficient of lateral earth pressure at rest (referred to as $K_0$) often relies on established classical equations. However, these equations often overlook the influence of the width of the backfill soil on lateral earth pressure. While this omission is generally acceptable when the backfill soil is wide enough, there are instances where a retaining wall supports backfill soils of limited width, such as basement walls between adjacent buildings. Yet, there is limited research addressing the impact of narrow backfill in such scenarios. We aimed to address this gap by investigating variations in $K_0$ values under different conditions, including backfill width and soil properties. Using ABAQUS for numerical simulations, we refined and validated our model using relevant laboratory experimental data. Subsequently, the validated model was applied to various simulation scenarios. For narrow backfill widths (ranging from 0.1 to 0.7 times the retaining wall height), our findings indicated a general decrease in $K_0$ values with decreasing backfill widths, often smaller than those estimated using classical equations. Additionally, along the depth of the wall, $K_0$ values tended to decrease with increasing depth for narrow backfill widths. These findings contribute to our understanding of the impact of narrow backfill on $K_0$.

**Keywords:** soil; lateral earth pressure; retaining wall; backfill width; finite element; at-rest condition

## 1. Introduction

In the context of urban expansion, retaining structures find widespread application in diverse settings, including building basements, roads, and rivers. When designing these structures, the lateral earth pressure is an important parameter to be determined, which is equal to the effective vertical stress multiplied by the lateral earth pressure coefficient ($K$). Depending on the movement of walls and their directions, this coefficient is categorized into active, passive, and at-rest earth pressure coefficients.

In practical applications, active and passive earth pressure coefficients are commonly computed because lateral wall movements are assumed to occur in most design scenarios. Therefore, a large body of existing research focuses on active and passive earth pressures acting on retaining structures. Common analysis methods include limit equilibrium [1–4], finite difference [5–7], and classical limit analysis methods [8–11]. However, some of these approaches rely on specific simplifications, such as pre-specified failure patterns, which may limit their applicability in more complex scenarios. Further insights into the non-linear distribution of active or passive earth pressures are offered by [12–17], presenting pseudo-dynamic approaches to assess the effects of various parameters such as soil-wall friction angle, soil friction angle, and sliding stability of retaining walls.

Nevertheless, there are instances characterized by neglectable lateral wall movements, such as laterally restrained basement walls situated between two adjacent buildings. In such cases, the application of the at-rest lateral earth pressure coefficient ($K_0$) is more suitable. The definition of $K_0$ is presented in Eq. 1. Various empirical equations have been proposed to calculate $K_0$ using mainly the angle of friction of soil. Jaky's equation, as shown in Eq. 2 [18], is the most widely utilized. Jaky's equation is a simplified form of Eq. 3, where the fraction term is omitted. Subsequent researchers have introduced modifications to Jaky's equation. Saglamer, through odometer tests on air-dried, uniform, cohesionless sandy soils from three different sites, derived a modified equation for $K_0$, as shown in Eq. 4 [19]. Considering sandy soils, Bolton proposed a fractional form in Eq. 5 [20]. To explore potential improvements on Jaky's equation, Szepeshazi conducted tests on various formulae using 153 measured data points, resulting in an optimized solution in Eq. 6 [21]. In addition to the angle of friction, efforts have also been made to understand the effect of various other factors on $K_0$, such as porosity, fragmentation process and elasticity modulus of granular materials [22,23], transverse strains [24,25].

$$K_0 = \frac{\sigma_h'}{\sigma_v'} \tag{1}$$

where $\sigma_h'$ and $\sigma_v'$ represent the effective lateral earth pressure and the effective vertical earth pressure, respectively.

$$K_0 = (1 - \sin\varphi) \tag{2}$$

$$K_0 = (1 - \sin\varphi)\frac{1 + \frac{2}{3}\sin\varphi}{1 + \sin\varphi} \tag{3}$$

$$K_0 = 0.97(1 - 0.97\sin\varphi) \tag{4}$$

$$K_0 = \frac{1-\sin\left(\varphi-11.5^\circ\right)}{1+\sin\left(\varphi-11.5^\circ\right)} \tag{5}$$

$$K_0 = 0.95\left(1-\sin\varphi\right) \tag{6}$$

The calculation of $K_0$ is conventionally performed under the assumption of an adequate width of soil behind a retaining wall. However, scenarios exist where the backfill soil width is restricted, notably in retaining walls situated in mountainous regions or urban build-up areas due to spatial constraints. A limited number of studies [26–30] have explored the impact of narrow backfill width on $K_0$.

Janssen's Arching Theory [31] suggested that the main distinction between unlimited and narrow backfill width was attributed to the reduction of pressures by soil-wall interaction. The wall's vertical friction prevents the upper soil layer from exerting its full weight on the layer below, resulting in a reduction in the resultant force in the vertical direction. Addressing this issue, Handy [29] proposed Eq. 7 through a theoretical approach to estimate the at-rest earth pressure coefficient under narrow backfill conditions.

$$K_0^{'} = \frac{1}{2\tan\varphi'}\frac{L}{z}\left[1-\exp\left(-2K_0\frac{z}{L}\tan\varphi'\right)\right] \tag{7}$$

where $L$ is the backfill width; $z$ is the ground depth; $\varphi'$ is the soil-wall friction angle; and $K_0$ is the classical at-rest earth pressure coefficient under an unlimited backfill width.

In addition to analytical and theoretical investigations, centrifuge experiments have been employed to examine lateral earth pressure on retaining structures [26,27,32]. Frydman and Keissar [26] utilized centrifuge tests to mimic retaining walls near rock faces under at-rest conditions. Investigating different aspect ratios (ratios of backfill width to wall height) ranging from 0.1 to 1.1, they observed a decrease in the measured $K_0$ values as the backfill width increased. A similar trend was noted in the centrifuge experiments conducted by Take and Valsangkar on rigid retaining walls [27].

Previous research on $K_0$ primarily leaned on theoretical frameworks [29], analyses [33], or experiments [26,27] that did not thoroughly explore the effect of different factors on $K_0$, particularly when dealing with narrow backfill widths. Consequently, the impact of narrow backfill width on $K_0$ remains uncertain. Hence, conducting comprehensive numerical simulations, capable of simulating and analyzing various variables, constitutes the primary contribution of this study.

## 2. Materials and methods

### *2.1. Key factors in numerical simulations*

Based on the related work on $K_0$ in Section 2, we seek to establish correlations between $K_0$ and key variables, including backfill widths $L$, wall depths $z$, and soil types of different properties. Soil properties considered include friction angle $\varphi$, cohesion $c$, modulus of elasticity $E$, and Poisson's ratio $\mu$.

### *2.2. Setup of finite element model*

Finite element modeling has proven to be a widely employed technique for modeling the stability of geo-structures with a variety of soil conditions [33–37], analyzing geosynthetic-reinforced retaining walls [38,39], evaluating the impact of varying environmental conditions on retaining structures, and analyzing soil-wall interactions [40–42], making it an appropriate tool for addressing the research problem in this study.

In this research, the finite element software ABAQUS is selected for implementing the intended numerical simulations. To create a validated finite element model, the parameters from the experimental study [26] are utilized to customize our ABAQUS model, ensuring its consistency with their experimental findings. The model setup, along with the associated soil parameters for validation, is depicted in Figure 1 and Table 1, based on data from [26]. Since the geometry in Figure 1(a) is symmetric, the finite element model in Figure 1(b) considers only half of it. Sections 3.2.1, 3.2.2, and 3.2.3 elaborate on the material components, meshes, and boundary conditions, respectively.

In addition to the parameters used for model establishment and validation, an extra validation is performed using laboratory test results in [27]. This supplementary validation considers the outcomes of Test B and Test D in [27], representing backfill widths of 75 mm and 15 mm, respectively. Once the ABAQUS model is validated, it is employed for various simulations where the values of key design variables are adjusted, as detailed in Section 3.3.

#### 2.2.1. Material Components

The initial ABAQUS model is constructed based on the data (comprising geometry, soil properties, and soil-wall friction coefficient) related to the retaining wall used in a series of centrifuge tests documented in [26]. These data aid in validating our model against experimental results. Figure 1 illustrates the wall with a height ($H$) of 160 mm and a width of 1 mm. The backfill has a width ($L$) of 45 mm, matching the wall's height and extending along its length. The wall body is represented as an isotropic and elastic material. The backfill soil is characterized using Mohr-Coulomb Plasticity, assuming perfect plasticity [41].

In our initial model built for validation, the internal friction angle ($\varphi$) of the backfill is set as 36° according to [26]. Regarding the soil-wall interaction, the following conditions are presumed. Initially, the wall is assumed to exhibit frictional behavior with a soil-wall friction coefficient of 0.364, as per [26]. For Elastic Slip at the wall-soil interface, the characteristic surface dimension fraction is set to infinitesimally small. Additionally, “Hard” Contact is selected for Pressure-Overclosure, indicating that separation between wall meshes and soil meshes at the contact surface is prohibited.

#### 2.2.2. Meshes

For meshing, the eight-node plane strain cell (CPE8) is employed. The approximate global size is configured at 0.2, with a maximum deviation factor set to 0.1. This meshing strategy results in a total of 10,681 nodes and 3,384 mesh elements.

### 2.2.3. Boundary conditions

The self-weight of the backfill is applied in the model, determined by a uniform soil density of 16.4 kN/m³. Boundary conditions (BC1 and BC2) are applied to the wall and backfill mesh nodes, respectively. BC1 restricts horizontal movements and rotations at the right edge of the model, while BC2 restricts vertical movements and rotations at the bottom edge of the model.

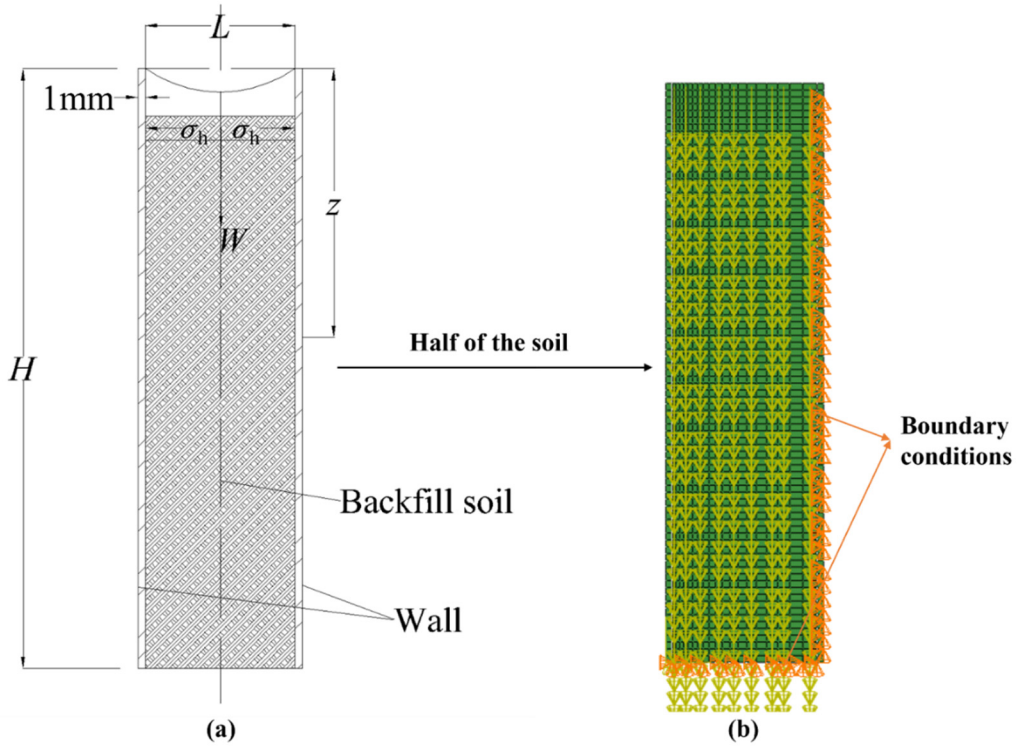


**Figure 1.** Illustration of the finite element model: (a) Geometry, and (b) load, meshes, and boundary conditions.

**Table 1.** Material properties used for model validation, according to [26].

| Material Components | Density (g/cm$^3$) | Modulus of elasticity (MPa) | Poisson's ratio | Friction angle (°) |
|---|---|---|---|---|
| Wall | - | $2 \times 10^{15}$ | 0.05 | - |
| Soil | 1.64 | 30 | 0.3 | 36 |

### *2.3. Key factors considered*

Using the validated finite element model, adjustments to the inputs are made to investigate the impact of backfill width and soil properties on the at-rest lateral earth pressure coefficient $K_0$. This approach allows for an in-depth exploration of how different backfill widths and soil types influence the at-rest lateral earth pressure coefficient. This study considers various backfill widths, specifically 1 m, 3 m, 5 m, 7 m, and 50 m, with a retaining wall height of 10 m. The corresponding normalized backfill widths ($L/H$ or aspect ratio) are 0.1, 0.3, 0.5, 0.7, and 5, respectively. It is assumed that $L/H = 5$ is sufficiently large, and any further increase in width would not influence the lateral earth pressure

in the model. The other normalized widths are employed to simulate the effects of finite backfill widths on $K_0$. We consider a variety of soils with distinct properties. Table 2 provides a summary of the soil parameters used in the simulations, sourced from the Geotechdata database [43].

**Table 2.** Soil properties considered in the simulations, according to [43].

| Soil types | Unit weight (kN/m$^3$) | Cohesion (kPa) | Friction angle (°) | Poisson's ratio | Modulus of elasticity (MPa) |
|---|---|---|---|---|---|
| Sandy gravels | 19 | 0 | 40 | 0.32 | 80 |
| Firm clay | 19 | 20 | 25 | 0.35 | 20 |
| Medium sand | 19 | 0 | 33 | 0.3 | 40 |

### *2.4. Sensitivity analysis*

Sensitivity analyses were conducted to investigate the impacts of different parameters in simulations, encompassing soil friction angle, soil-wall friction angle (derived as 2/3 times the soil friction angle), modulus of elasticity, Poisson's ratio, and cohesion. The ranges of values for these parameters were systematically tested in our sensitivity analyses, as depicted in Table 3.

**Table 3.** Range of values of the soil parameters considered in sensitivity analyses.

| Sensitivity Analysis Tests | Unit weight (kN/m$^3$) | Cohesion (kPa) | Soil friction angle (°) | Poisson's ratio | Modulus of elasticity (MPa) |
|---|---|---|---|---|---|
| Test 1 | 19 | 0 | 25, 30, 35, 40, 45 | 0.3 | 40 |
| Test 2 | 19 | 0 | 35 | 0.1, 0.2, 0.3,0.4, 0.5 | 40 |
| Test 3 | 19 | 0 | 35 | 0.3 | 1, 5, 10, 20, 80 |
| Test 4 | 19 | 1, 5, 10, 20, 40 | 35 | 0.3 | 40 |

## 3. Results

### *3.1. Model validation*

Figure 2 displays the variations in lateral earth pressure coefficients with wall depth, incorporating data from our ABAQUS simulations conducted under at-rest conditions, Frydman and Keissar's experimental tests, Jaky's equation (Eq. 2), and the arching equation (Eq. 7). Theoretically, $K_0$ values should surpass those of $K_\mathrm{a}$ (i.e., the active lateral earth pressure coefficient). To confirm this, $K_\mathrm{a}$ values were calculated using Coulomb's method, as indicated in Eq. 8 [44], assuming flat backfill and vertical walls, and are presented in Figure 2 for comparison. Despite some disparities at the upper and lower wall depths, the $K_0$ values corresponded with those derived from the arching equation and exhibited a similar trend to that observed in the experiments conducted by Frydman and Keissar [26].

$$K_a = \frac{\cos^2 \varphi}{\cos \varphi' \left[ 1 + \sqrt{\frac{\sin(\varphi + \varphi') \sin \varphi}{\cos \varphi'}} \right]^2} \tag{8}$$

where $\varphi$ is the soil friction angle and $\varphi'$ is the soil-wall friction angle.

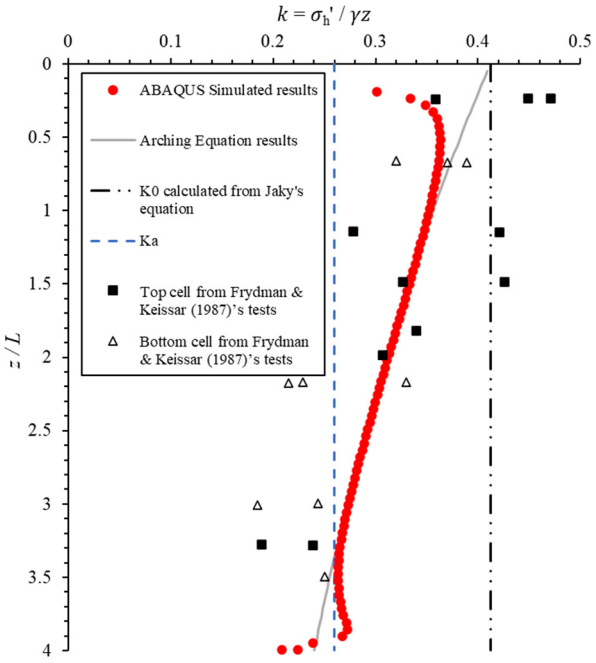


**Figure 2.** Comparisons in lateral earth pressure coefficients estimated by our finite element model and other methods (including the centrifuge tests of [26], the arching equation (Eq. 7), the Jaky's equation [18] and the Rankine's active earth pressure coefficient) where the depth is normalized as $z/L$ ($z$ is the depth from the wall crest and $L$ is the backfill width).

In Figure 3, the lateral earth pressure estimated from our finite element simulations was compared with the test results from Take and Valsangkar [27]. The visual inspection further confirms the accurate prediction capabilities of our finite element model concerning lateral earth pressure.

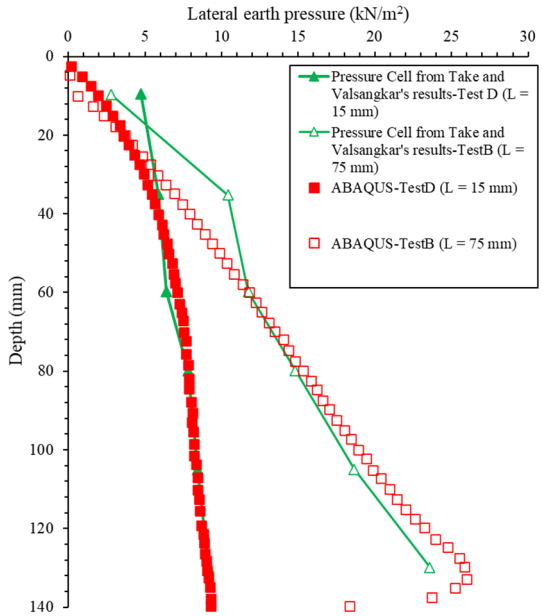


**Figure 3.** Comparisons in lateral earth pressures versus depth, estimated by our finite element model and the centrifuge test results of Take and Valsangkar [27].

### *3.2. Effects of backfill widths and soil properties on $K_0$*

Figure 4 presents the variations in $K_0$ values with wall depth at different aspect ratios for various soils. As observed, the backfill width exerted a substantial impact on $K_0$ values. On average, there was a decrease in $K_0$ values as the width of narrow backfill decreased. This effect is more pronounced at smaller aspect ratios (e.g., $L/H = 0.1$ to $L/H = 0.3$), with a reduced impact observed as the aspect ratio increased (e.g., from $L/H = 0.5$ to $L/H = 0.7$). With respect to the narrow backfill widths, the changes in $K_0$ over the wall depth exhibited a nonlinear decrease at smaller aspect ratios, transitioning to more uniform values with increasing aspect ratios. This trend was consistent across various soil types considered in the study. Such variations in $K_0$ with the wall depth was likely attributed to the soil-wall friction. To confirm this, Figure 4(d) shows the simulated $K_0$ values for medium sands when zero soil-wall friction was considered. Under this condition, almost constant $K_0$ values were observed. In addition, the effect of backfill width was significantly reduced, although a smaller backfill width also led to a slightly smaller $K_0$ values. In addition, all simulated $K_0$ values for clays and granular soils corresponded well to laboratory experiment results by Mesri and Hayat [25], where $K_0$ values for soft plastic cohesive soil were found to be between 0.31~0.67.

Furthermore, Figure 4 also presents $K_0$ values estimated using Eq. (2) and Eqs. (4)–(6) as benchmark values representing conditions with adequately wide backfill widths. These benchmarks, along with the $K_a$ values calculated by Eq. (8), were compared with $K_0$ values predicted by our finite element models. Notably, the Saglamer's and Bolton's equations were applicable only to sandy materials and were excluded for calculating $K_0$ for firm clay. For medium sand and firm clay, the predicted $K_0$ values at various backfill widths were smaller than the benchmark values. For sandy gravels, the predicted $K_0$ values were either slightly smaller or larger than benchmark values, depending on the backfill width.

Figure 4 shows that $K_0$ values at the aspect ratio $L/H = 0.1$ varied significantly with wall depth, likely attributing to soil-wall friction and exceptionally small aspect ratio. Under this small aspect ratio, $K_0$ values at certain depths were smaller than $K_a$ values, contradicting the conventional theoretical expectation that $K_0$ values should surpass $K_a$ values for a given soil. The exact reasons for this deviation remain unclear, demanding future investigations. However, $K_0$ values obtained from the numerical simulations may not be directly comparable to $K_a$ values calculated using the theoretical equation, as the theoretical solution does not involve the complex set of parameters considered in the simulations. In addition, the engineering significance of this deviation is minimal, given the rarity of encountering a retaining wall with such a small aspect ratio.

For narrow backfill widths, the predicted $K_0$ values near the crest of the wall displayed a concave-downward trend, likely attributed to the effect of boundary condition, especially soil-wall friction, which constrained vertical backfill movements and may unrealistically represent actual backfill behavior.

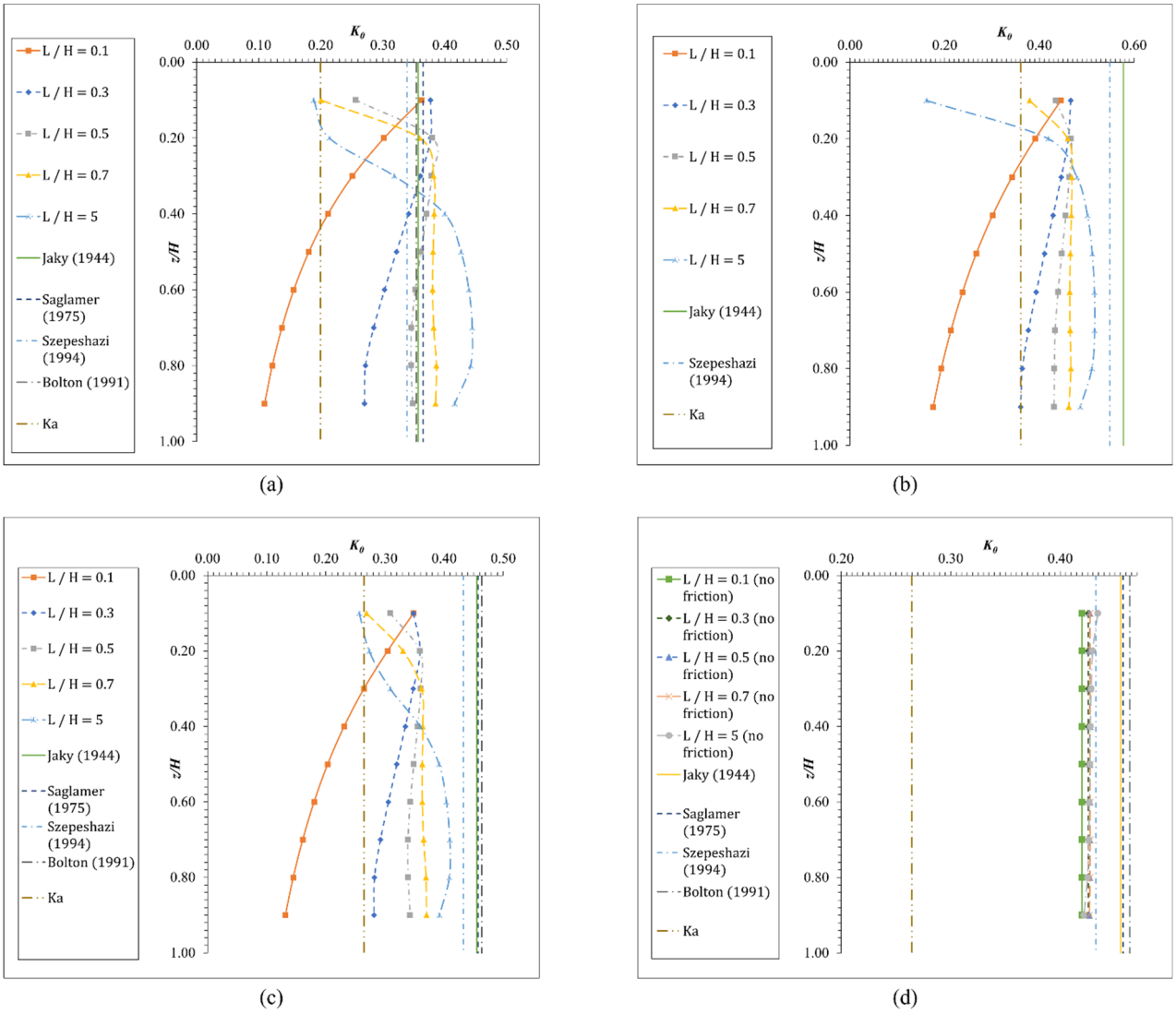


**Figure 4.** Variations in $K_0$ values with wall depth and aspect ratio: (a) Sandy gravels with soil-wall friction taken into account, (b) firm clay with soil-wall friction taken into account, (c) medium sand with consideration of soil-wall friction, and (d) medium sand without consideration of soil-wall friction.

### *3.3. Sensitivity analysis*

The analysis findings reveal that the $K_0$ values derived from our model were almost not affected by cohesion and modulus of elasticity, as shown in Figure 5. However, they exhibited significant variations with soil friction angle and Poisson's ratio, as depicted in Figure 6 for $L/H = 0.1$ and Figure 7 for $L/H = 0.7$. A higher soil internal friction angle corresponded to a decrease in $K_0$ values, whereas a higher Poisson's ratio resulted in an increase in $K_0$ values.

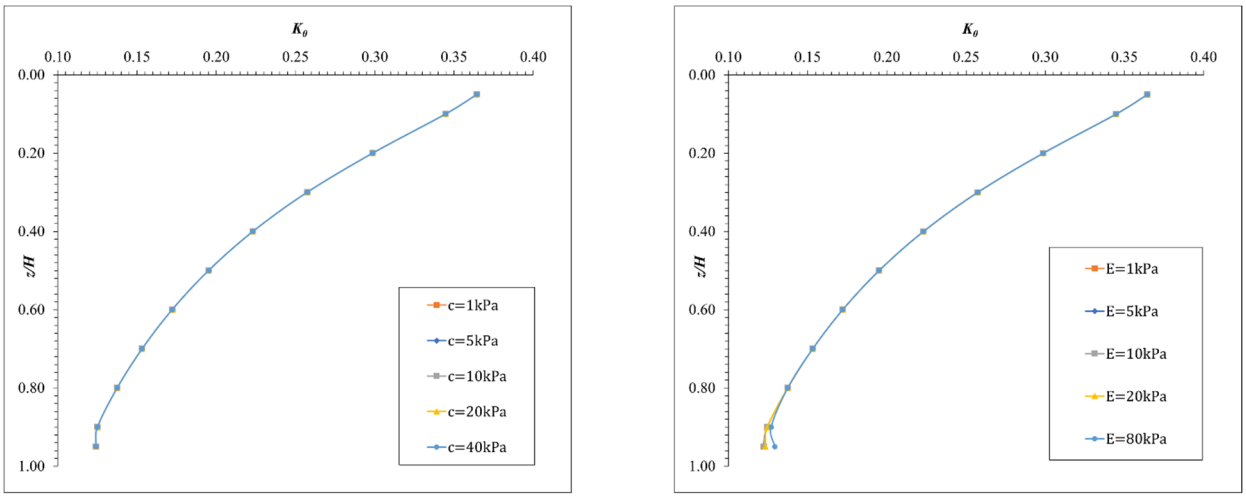


**Figure 5.** Factors that the model is not sensitive to under narrow backfill width (using under $L/H = 0.1$ as an example): (a) Variations in $K_0$ values with cohesion and (b) Variations of $K_0$ values with modulus of elasticity.

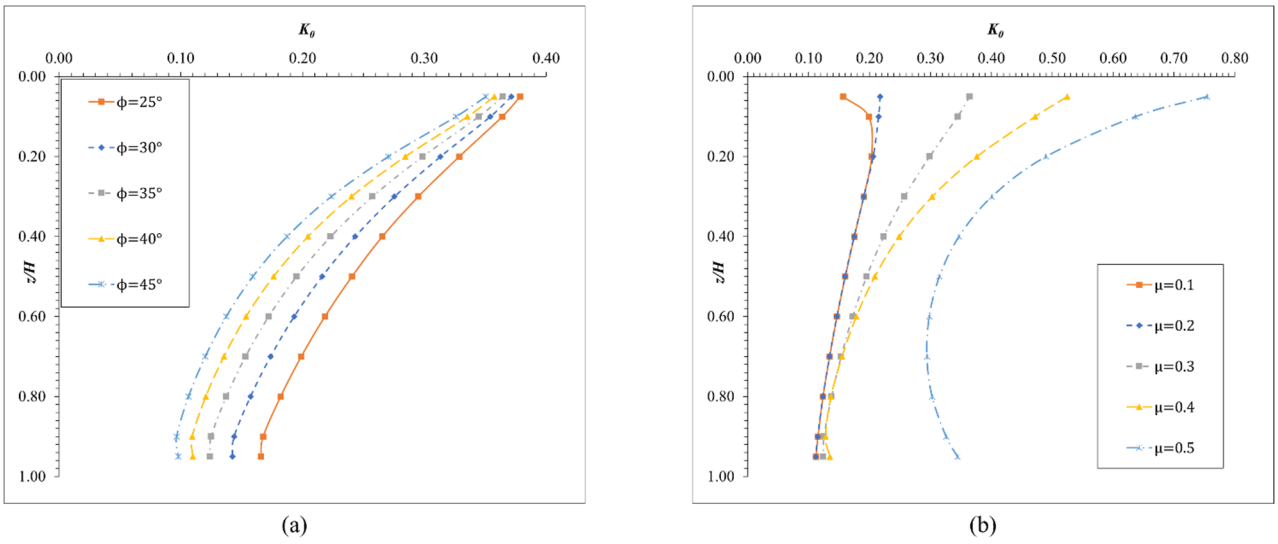


**Figure 6.** Factors that the model is sensitive to under narrow backfill with consideration of soil-wall friction (using $L/H = 0.1$ as an example): (a) Variation in $K_0$ values with soil friction angle and (b) variation in $K_0$ values with Poisson's ratio.

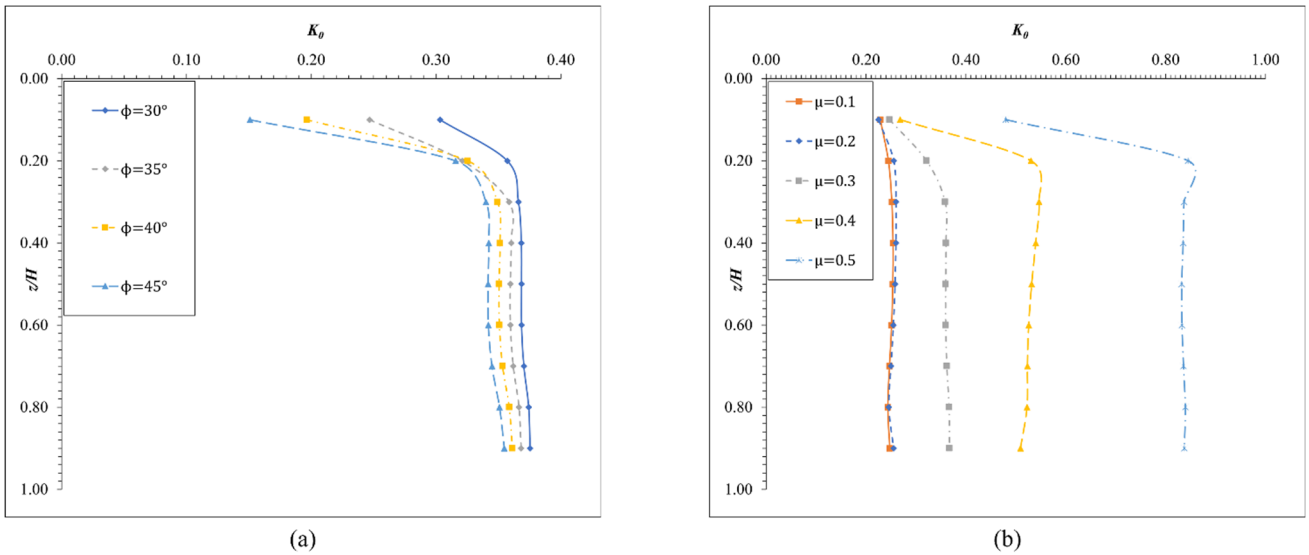


**Figure 7.** Factors that the model was sensitive to under narrow backfill width with consideration of soil-wall friction (using $L/H = 0.7$ as an example): (a) Variation in $K_0$ values with soil friction angle and (b) variation in $K_0$ values with Poisson's ratio.

### *3.4. Simulation of the displacement field and strain field*

Figure 8 displays the horizontal displacement field of soils at the soil-wall interface from the simulations under the narrow backfill width $L/H = 0.1$. The values of displacement increased as the soil depth increased. Additionally, likely due to its comparatively large value of Poisson's ratio, the largest displacements were observed for firm clay amongst all the three soils considered.

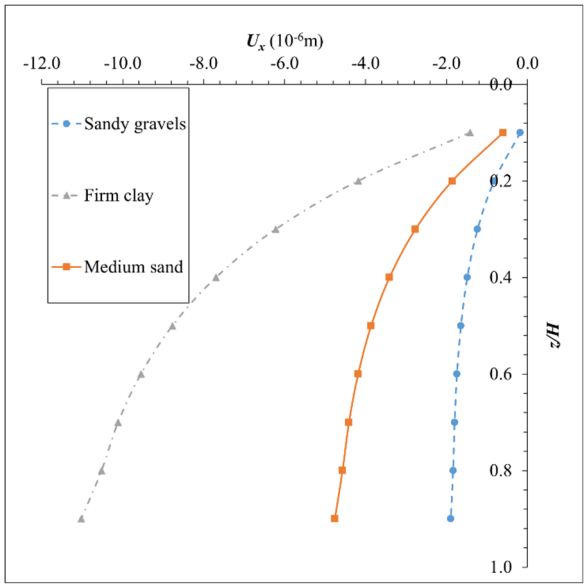


**Figure 8.** Lateral displacements for different soils considered, under narrow backfill widths (using $L/H = 0.1$ as an example).

## 4. Discussion

A primary limitation within numerical modeling is the oversimplified representation of material properties. Our model assumed a homogeneous material behavior, disregarding the inherent heterogeneity found in natural soils and backfill materials. Lade and Duncan's studies [45] underscored the impact of material heterogeneity on the emergence of localized failure mechanisms within the backfill. Moreover, the assumption of soils as continuum materials in finite element modeling fails to adequately capture their granular nature, especially concerning sands and gravels. Hence, as a prospective direction for further research, it is interesting to investigate the variation of $K_0$ under diverse conditions utilizing a discrete element modeling approach [46–48].

The accuracy of numerical models significantly relies on the accurate representation of boundary conditions. The interaction between the retaining wall and the surrounding soil constitutes a complex and dynamic process. However, accurately modeling this interaction is challenging, which may have limited the overall performance of our models. Numerical models typically adopt simplified approaches to depict this interaction. Such oversimplification may yield inaccurate predictions regarding wall stability and deformation behavior, particularly in cases of narrow backfill width. Researchers have [49] illustrated that improper boundary conditions can lead to distorted pressure distributions and erroneous forecasts of wall deformation behavior. Several prior studies [50,51] have demonstrated that the Goodman contact element proves more suitable for the soil-wall interface. Nevertheless, their findings are confined to specific scenarios such as cantilever or masonry walls, leaving suitable contact models for our investigated problem to be further explored.

Construction methods can markedly impact the stress state and deformation behavior of narrow backfill width retaining walls [52]. For instance, inadequacies in backfilling procedures or insufficient compaction efforts may result in non-uniform soil density and lateral pressure distribution, thereby influencing the overall performance and serviceability of the retaining wall. Failure to replicate these interactions in numerical models may result in underestimation of long-term deformations of retaining walls.

Research conducted by [53] showcased that the presence of surcharge loading can modify the distribution of lateral earth pressures on retaining walls. This redistribution may result in localized stress concentrations and potential failure mechanisms, particularly near the top of the wall where surcharge loading is most pronounced. Additionally, surcharge loading can influence the emergence of critical failure surfaces within the backfill, thereby impacting the overall stability of the retaining wall system [54].

## 5. Conclusions

In this study, we employed numerical simulations with the ABAQUS finite element software to predict the at-rest lateral earth pressure coefficient ($K_0$) for various backfill widths in a retaining structure. The crucial parameters considered were the ratio of backfill width to wall depth ($L/H$) and soil properties. The model underwent refinement and validation using experimental results documented in the literature. Subsequently, the validated finite element model, with adjusted parameter values, was applied to various test cases.

For the narrow backfill widths investigated ($L/H = 0.1, 0.3, 0.5$ and $0.7$), our findings revealed a consistent decrease in $K_0$ values on average as the backfill width decreased, suggesting that

conventional equations likely overestimate lateral earth pressures in the case of a narrow backfill width. This trend was observed across all three soil types examined. Additionally, it was noted that the values of $K_0$ exhibited a nonlinear decrease with depth when the ratio of backfill width to wall depth was small. These findings underscored a deficiency in classical equations, which offer a constant value of $K_0$ irrespective of backfill width and depth. Within our model, the inclusion of soil-wall friction and Poisson's ratio emerged as critical factors influencing the variability of simulated $K_0$ values across diverse conditions. Interestingly, in instances where soil-wall friction was disregarded, $K_0$ values exhibited minimal alterations with depth.

## Use of AI tools declaration

The authors declare that they have not used Artificial Intelligence (AI) tools in the creation of this article.

## Acknowledgments

This research was funded by Suzhou Huihu Lixin Education Development Foundation, with grant number RDS10120230055.

## Conflict of interest

There are no identified conflicts of interest.

## References

1. Bathurst R, Cai Z (1995) Pseudo-static seismic analysis of geosynthetic-reinforced segmental retaining walls. *Geosynth Int* 2: 787–830. https://doi.org/10.1680/gein.2.0037
2. Leshchinsky D, Leshchinsky B, Leshchinsky O (2017) Limit state design framework for geosynthetic-reinforced soil structures. *Geotextiles Geomembranes* 45: 642–652. https://doi.org/10.1016/j.geotexmem.2017.08.005
3. Pain A, Choudhury D, Bhattacharyya S (2017) Effect of dynamic soil properties and frequency content of harmonic excitation on the internal stability of reinforced soil retaining structure. *Geotextiles Geomembranes* 45: 471–486. https://doi.org/10.1016/j.geotexmem.2017.07.003
4. Steedman R, Zeng X (1990) The influence of phase on the calculation of pseudo-static earth pressure on a retaining wall. *Geotechnique* 40: 103–112. https://doi.org/10.1680/geot.1990.40.1.103
5. Huang J, Parsons RL, Han J, et al. (2011) Numerical analysis of a laterally loaded shaft constructed within an MSE wall. *Geotextiles Geomembranes* 29: 233–241. https://doi.org/10.1016/j.geotexmem.2010.11.003
6. Bathurst R, Hatami K (1998) Seismic response analysis of a geosynthetic-reinforced soil retaining wall. *Geosynth Int* 5: 127–166. https://doi.org/10.1680/gein.5.0117
7. Zheng Y, Fox PJ, McCartney JS (2018) Numerical simulation of deformation and failure behavior of geosynthetic reinforced soil bridge abutments. *J Geotech Geoenviron* 144: 04018037. https://doi.org/10.1061/(ASCE)GT.1943-5606.0001893

8. Garcia-Suarez J, Asimaki D (2020) Exact seismic response of smooth rigid retaining walls resting on stiff soil. *Int J Numer Anal Met* 44: 1750–1769. https://doi.org/10.1002/nag.3082
9. Mojallal M, Ghanbari A, Askari F (2012) A new analytical method for calculating seismic displacements in reinforced retaining walls. *Geosynth Int* 19: 212–231. https://doi.org/10.1680/gein.2012.12.00010
10. Xie Y, Leshchinsky B, Yang S (2016) Evaluating reinforcement loading within surcharged segmental block reinforced soil walls using a limit state framework. *Geotextiles Geomembranes* 44: 832–844. https://doi.org/10.1016/j.geotexmem.2016.06.010
11. Leshchinsky D, Kang B, Han J, et al. (2014) Framework for limit state design of geosynthetic-reinforced walls and slopes. *Transp Infrastruct Geotechnol* 1: 129–164. https://doi.org/10.1007/s40515-014-0006-3
12. Mylonakis G, Kloukinas P, Papantonopoulos C (2007) An alternative to the Mononobe–Okabe equations for seismic earth pressures. *Soil Dyn Earthq Eng* 27: 957–969. https://doi.org/10.1016/j.soildyn.2007.01.004
13. Choudhury D, Nimbalkar S (2007) Seismic rotational displacement of gravity walls by pseudo-dynamic method: Passive case. *Soil Dyn Earthq Eng* 27: 242–249. https://doi.org/10.1016/j.soildyn.2006.06.009
14. Choudhury D, Nimbalkar S (2005) Seismic passive resistance by pseudo-dynamic method. *Geotechnique* 55: 699–702. https://doi.org/10.1680/geot.2005.55.9.699
15. Nimbalkar S, Choudhury D (2007) Sliding stability and seismic design of retaining wall by pseudo-dynamic method for passive case. *Soil Dyn Earthq Eng* 27: 497–505. https://doi.org/10.1016/j.soildyn.2006.11.006
16. Choudhury D, Nimbalkar SS (2006) Pseudo-dynamic approach of seismic active earth pressure behind retaining wall. *Geotech Geol Eng* 24: 1103–1113. https://doi.org/10.1007/s10706-005-1134-x
17. Eskandarinejad A, Shafiee A (2011) Pseudo-dynamic analysis of seismic stability of reinforced slopes considering non-associated flow rule. *J Cent South Univ T* 18: 2091–2099. https://doi.org/10.1007/s11771-011-0948-3
18. Jaky J (1944) The coefficient of earth pressure at rest. *J Soc Hung Archit Eng*.
19. Saglamer A (1975) Soil parameters affecting coefficient of earth pressure at rest of cohesionless soils. In Proceedings of Istanbul conference on soil/mechanics and Foundation Engineering, Istanbul, Turkey, 9–16.
20. Bolton MD (2013) A guide to soil mechanics: Universities Press. https://doi.org/10.1007/978-1-349-16208-6
21. Szepeshazi R (1994) ON THE $K_0$ FACTOR. *Period Polytech Civ Eng* 38: 127–135.
22. Schöpfer MP, Abe S, Childs C, et al. (2009) The impact of porosity and crack density on the elasticity, strength and friction of cohesive granular materials: Insights from DEM modelling. *Int J Rock Mech Min Sci* 46: 250–261. https://doi.org/10.1016/j.ijrmms.2008.03.009
23. Rad AB (2018) Static analysis of non-uniform 2D functionally graded auxetic-porous circular plates interacting with the gradient elastic foundations involving friction force. *Aerosp Sci Technol* 76: 315–339. https://doi.org/10.1016/j.ast.2018.01.036
24. Cornforth DH (1964) Some experiments on the influence of strain conditions on the strength of sand. *Geotechnique* 14: 143–167. https://doi.org/10.1680/geot.1964.14.2.143

25. Mesri G, Hayat T (1993) The coefficient of earth pressure at rest. *Can Geotech J* 30: 647–666. https://doi.org/10.1139/t93-056
26. Frydman S, Keissar I (1987) Earth pressure on retaining walls near rock faces. *J Geotech Eng* 113: 586–599. https://doi.org/10.1061/(ASCE)0733-9410(1987)113:6(586)
27. Take W, Valsangkar A (2001) Earth pressures on unyielding retaining walls of narrow backfill width. *Can Geotech J* 38: 1220–1230. https://doi.org/10.1139/t01-063
28. Kniss KT, Yang KH, Wright SG, et al. (2007) Earth pressures and design considerations of narrow MSE walls. Proc Texas Section ASCE Spring 2007. Available from: https://sites.utexas.edu/zornberg/files/2022/03/Kniss_Yang_Wright_Zornberg_2007.pdf.
29. Handy RL (1985) The arch in soil arching. *J Geotech Eng* 111: 302–318. https://doi.org/10.1061/(ASCE)0733-9410(1985)111:3(302)
30. Aggour M, Brown C (1974) The prediction of earth pressure on retaining walls due to compaction. *Geotechnique* 24: 489–502. https://doi.org/10.1680/geot.1974.24.4.489
31. Janssen H (1895) Versuche uber getreidedruck in silozellen. *Z ver deut Ing* 39: 1045.
32. Woodruff R (2003) Centrifuge modeling for MSE-shoring composite walls: University of Colorado.
33. Safardoost Siahmazgi A, Fathipour H, Jamshidi Chenari R, et al. (2022) Evaluation of the pseudo-dynamic bearing capacity of surface footings on cohesionless soils using finite element lower bound limit analysis. *Geomech Geoeng* 17: 765–777. https://doi.org/10.1080/17486025.2021.1889686
34. Fathipour H, Tajani SB, Payan M, et al. (2022) Influence of transient flow during infiltration and isotropic/anisotropic matric suction on the passive/active lateral earth pressures of partially saturated soils. *Eng Geol* 310: 106883. https://doi.org/10.1016/j.enggeo.2022.106883
35. Fathipour H, Payan M, Jamshidi Chenari R, et al. (2021) Lower bound analysis of modified pseudo-dynamic lateral earth pressures for retaining wall-backfill system with depth-varying damping using FEM-Second order cone programming. *Int J Numer Anal Met* 45: 2371–2387. https://doi.org/10.1002/nag.3269
36. Fathipour H, Siahmazgi AS, Payan M, et al. (2020) Evaluation of the lateral earth pressure in unsaturated soils with finite element limit analysis using second-order cone programming. *Comput Geotech* 125: 103587. https://doi.org/10.1016/j.compgeo.2020.103587
37. Fathipour H, Siahmazgi AS, Payan M, et al. (2021) Limit analysis of modified pseudodynamic lateral earth pressure in anisotropic frictional medium using finite-element and second-order cone programming. *Int J Geomech* 21: 04020258. https://doi.org/10.1061/(ASCE)GM.1943-5622.0001924
38. Mirmoazen SM, Lajevardi SH, Mirhosseini SM, et al. (2021) Active lateral earth pressure of geosynthetic-reinforced retaining walls with inherently anisotropic frictional backfills subjected to strip footing loading. *Comput Geotech* 137: 104302. https://doi.org/10.1016/j.compgeo.2021.104302
39. Fathipour H, Payan M, Chenari RJ (2021) Limit analysis of lateral earth pressure on geosynthetic-reinforced retaining structures using finite element and second-order cone programming. *Comput Geotech* 134: 104119. https://doi.org/10.1016/j.compgeo.2021.104119
40. Yang KH, Liu CN (2007) Finite element analysis of earth pressures for narrow retaining walls. *J Geoeng* 2: 43–52. Available from: http://yo-1.ct.ntust.edu.tw/jge/files/articlefiles/v2i2200709051462998162.pdf.

41. Helwany S (2007) Applied soil mechanics with ABAQUS applications: John Wiley & Sons. https://doi.org/10.1002/9780470168097
42. Li L, Aubertin M, Simon R, et al. (2003) Modeling arching effects in narrow backfilled stopes with FLAC. Flac and numerical modeling in geomechanics: 211–219. Available from: https://api.semanticscholar.org/CorpusID:115066222
43. Geotechdata (2023) Geotechnical Parameters. pp. Designed by Geotechdata.info. Developed by Nuevvo. Available from: https://www.geotechdata.info/.
44. Motta E (1994) Generalized Coulomb active-earth pressure for distanced surcharge. *J Geotech Eng* 120: 1072–1079. https://doi.org/10.1061/(ASCE)0733-9410(1994)120:6(1072)
45. Lade PV, Duncan JM (1975) Elastoplastic stress-strain theory for cohesionless soil. *J Geotech Eng Divi* 101: 1037–1053. https://doi.org/10.1061/AJGEB6.0000204
46. Kodicherla SPK, Gong G, Fan L, et al. (2018) Effects of preparation methods on inherent fabric anisotropy and packing density of reconstituted sand. *Cogent Eng* 5: 1533363. https://doi.org/10.1080/23311916.2018.1533363
47. Kodicherla SPK, Gong G, Yang Z, et al. (2019) The influence of particle elongations on direct shear behaviour of granular materials using DEM. *Granular Matter* 21: 86. https://doi.org/10.1007/s10035-019-0947-x
48. Kodicherla SPK, Gong G, Fan L, et al. (2020) Investigations of the effects of particle morphology on granular material behaviors using a multi-sphere approach. *J Rock Mech Geotech Eng* 12: 1301–1312. https://doi.org/10.1016/j.jrmge.2020.04.005
49. Das BM, Sobhan K (1990) Principles of geotechnical engineering. Available from: http://faculty.tafreshu.ac.ir/file/download/course/1583609876-principles-of-geotechnical-engineering-8th-das.pdf
50. Goh AT (1993) Behavior of cantilever retaining walls. *J Geotech Eng* 119: 1751–1770. https://doi.org/10.1061/(ASCE)0733-9410(1993)119:11(1751)
51. Harkness R, Powrie W, Zhang X, et al. (2000) Numerical modelling of full-scale tests on drystone masonry retaining walls. *Géotechnique* 50: 165-179. https://doi.org/10.1680/geot.2000.50.2.165
52. Rowe RK, Skinner GD (2001) Numerical analysis of geosynthetic reinforced retaining wall constructed on a layered soil foundation. *Geotextiles Geomembranes* 19: 387–412. https://doi.org/10.1016/S0266-1144(01)00014-0
53. Helwany S, Reardon G, Wu J (1999) Effects of backfill on the performance of GRS retaining walls. *Geotextiles Geomembranes* 17: 1–16. https://doi.org/10.1016/S0266-1144(98)00021-1
54. Rao P, Chen Q, Zhou Y, et al. (2016) Determination of active earth pressure on rigid retaining wall considering arching effect in cohesive backfill soil. *Int J Geomech* 16: 04015082. https://doi.org/10.1061/(ASCE)GM.1943-5622.0000589


AIMS Press